Table of contents **Page**

Supplementary methods and results

Rhizophagus irregularis biomass processing, cell wall preparation, CN and FTIR analyses

The fungal biomass was extracted from root-free compartments of the monoxenic cultivation vessels filled with standard MSR medium amended with 1% sucrose and solidified or not with 0.5% Phytagel as described by Cranenbrouck et al. (2005). After solubilization of the solid medium in 10 mM citrate buffer (pH 6.0) for 20 min, the fungal biomass was washed on a 40 µm sieve with deionized water and then dried at 65°C for 48 hours. Fungal biomass from liquid cultures was washed on the sieve directly without extensive incubation in the citrate buffer. The AM fungal biomass was used for CN elemental analysis using a Flash EA 2000 instrument (Thermo Fisher Scientific, Waltham, MA, USA), analyzing samples weighing between 1500 and 2500 µg (results shown in Table S2). These analyses yielded total organic C and total N concentrations. Because experimental treatment of the mycorrhizal fungal biomass with citrate buffer did not yield different C and/or N concentrations in the samples (details not shown here), we present results from different fungal biomass samples (produced in liquid or solid cultivation media) together.

The fungal biomass samples (about 100 mg dry weight each) were homogenized in a ceramic mortar in 4 mL of chloroform-methanol mixture (2:1, v:v, Folch et al. 1957) for 5 min, centrifuged at 20000 g for 10 min, the pellets washed (in the following sequence) with 100% ethanol, 50% ethanol and ultrapure water, and finally dried in a vacuum centrifuge. This material was then subjected to both CN analysis (results shown in Table S2) and Fourier transformed infrared spectroscopy (FTIR). For the FTIR analyses, samples weighing 1 mg were analyzed using a Nicolet iS5 spectrometer (Thermo Scientific, Waltham, MA, USA) equipped with an attenuated total reflectance diamond tip adapter (iD7 ATR). Samples were measured to determine characteristic peaks related to bond stretching and rocking (Bernal-Ballen et al. 2019). Each spectrum represents 30 co-added scans referenced against an empty ATR cell spectrum. The FTIR analysis was carried out over a wave number range between 4000 cm^{-1} and 400 cm^{-1} at a resolution below 2 cm^{-1}. The spectra generated for the mycorrhizal fungal samples were compared to standard materials (microcrystalline cellulose, crab-shell chitin, bovine serum albumin, N-acetyl-glucosamine, and hyaluronic acid) obtained from Sigma-Aldrich (at least p.a. grade), and to purified cell walls from a zygomycete *Zygorrhynchus* sp. (Bukovská et al. 2018).

The resulting materials derived from the mycorrhizal fungal biomass were further milled in a ball mill (Retsch MM200, Retsch, Haan, Germany), using 5 mm zircon balls in 2-mL Eppendorf tubes to a fine powder and subjected to alkaline lysis (2% NaOH, 80°C, 3 hours) before washing the solid remnants with 100% ethanol, 100% acetone and ultrapure water (in this sequence) and drying the samples in a vacuum centrifuge. These samples were again subjected to CN and FTIR analyses (results shown in Table S2 and Figures S7-S9).

Trypsin digestion of cell walls obtained from *Rhizophagus irregularis* biomass

Aliquots of 10 - 30 mg of crab shell chitin or fungal (*Zygorrhynchus* or *Rhizophagus*) cell walls after alkaline lysis were treated with trypsin.This was done to expose chitin possibly hidden by proteins/peptides in the cell wall samples for further chitinase digestion. Crystalline trypsin from bovine pancreas was used for this purpose. It was provided by VWR (Stříbrná Skalice, Czech Republic), catalogue number M150-1G (2500 U mg^{-1}). The trypsin was dissolved so as to reach a concentration of 3 mg mL^{-1} in 1 mM HCl. The digestion was carried out in 100 mM Tris buffer (pH 8.5), maintaining the ratio 1:20 between the treated materials and trypsin (w:w), at 37°C for 24 h. Thereafter, the solid material was separated from the supernatant by centrifugation, and

subsequently washed with fresh 100 mM Tris buffer and three times with water, before being dried in a vacuum centrifuge.

Chitinase treatment

The samples treated previously with trypsin (i.e., dry weights between 10 and 30 mg) were further incubated with 0.5 U chitinase from *Clostridium thermocellum* (Megazyme, Ireland) in 1.5 ml of 50 mM phosphate/citrate buffer (pH 6.0) at 50 °C for three days. Each 24 h of incubation, 30 µL aliquots of the reaction mixtures were sampled, boiled at 99 °C for 3 min, centrifuged (10 min, 12000 g) and 20 µL of the resulting supernatants were used as samples for high-resolution liquid chromatography (HPLC) and liquid chromatography-mass spectrometry (LCMS) analyses.

HPLC and LCMS analyses

The HPLC analysis were carried out on a Shimadzu instrument described previously (Bojarová et al. 2017), using a HILCpak VN-50 4D column (5 µm, 150 × 4.6 mm) equipped with a guard column HILICpak VN-50G 4A (5 µm, 10 × 4.6 mm, both columns provided by Shodex, Showa Denko K.K., Japan) under binary gradient elution (mobile phase: A = acetonitrile; B = water; gradient: 0 min 22% B, 10 min 38% B, 12 min 22% B, 15 min stop), flow rate 1 mL min^{-1}, t = 60°C. The photometric diode array data were acquired in the 200–400 nm range, using a sampling frequency of 40 Hz, and signals at 200 nm were extracted. The injection volume was 1 µL. Retention time of *N*,*N*´-diacetylchitobiose was 4.107 min, whereas that of *N*, *N*´, *N*´´-triacetylchitotriose was 5.070 min. Results are shown in supplementary Tables S3 and S4.

The LCMS analyses were done on the same column and under the same conditions as described above, only the time for equilibration of the column was extended (by 5 min) because of a lower flow rate (0.4 mL min^{-1}) in this method. The MS parameters were as follows: positive mode; ESI interface voltage, 4.5 kV; detector voltage, 1.15 kV; nebulizing gas flow 1.5 mL min^{-1}; drying gas flow 15 mL min^{-1}; heat block temperature 200°C; DL temperature 250 °C; SCAN mode 450-700 m/z. Spectra were extracted using LabSolutions software version 5.75 SP2 (Shimadzu, Kyoto, Japan). Mass spectra of chitobiose and chitotriose from *Rhizophagus irregularis* are shown in supplementary Figures S10 and S11, respectively.

High resolution mass spectrometry of the methanolic extracts from AM fungal biomass

An LTQ-Orbitrap Velos mass spectrometer (Thermo Fisher Scientific, San Jose, CA, USA) equipped with a heated electrospray interface was operated in negative ionization mode. The MS scan was performed in the FT cell and recorded within a window between 200–4000 m/z. The mass resolution was set to 105,000, and the ion spray voltage was set at -2.5 kV in the negative ionization mode. The ionization mode used the following parameters: sheath gas flow, 18 arbitrary units (AU); auxiliary gas flow, 7 AU; ion source temperature, 250 °C; capillary temperature, 230 °C; capillary voltage, 50 V; and tube lens voltage, 170 V. Helium was used as a collision gas for collision-induced dissociation (CID) experiments. The CID normalization energy of 35% was used for the fragmentation of parent ions. The calibration of the MS was conducted with a Pierce LTQ Orbitrap negative ion calibration solution (provided by Thermo Fisher Scientific, San Jose, CA, USA). The internal lock mass was used in mass spectra acquisition, i.e., 255.2330 m/z [M-H]- palmitic acid in the negative ionization mode. The mass accuracy was better than 2 ppm. The chemical structure of the compounds was confirmed with the help of the spectral database (http://www.lipidmaps.org/) and by tandem MS.

Among many thousand compounds recorded in the MS analyses (details not shown), all classes of phosphatidyl-myo-inositol mannosides (PIMs) were identified. Phosphatidyl-myo-inositol mono-, di-, tri-, tetra-, penta-, and hexamannosides were denoted as PIM_1, PIM_2, PIM_3, PIM_4, PIM_5, and PIM_6,

respectively, where PIM represents the glycerol backbone substituted with two fatty acids. The conventional nomenclature described previously (Hsu et al. 2007a, b) was used for other phosphatidyl-myo-inositol mannosides derivatives having the abbreviations lyso-PIMs, PIMs, monoacyl-PIMs (Ac_1PIMs, i.e., triacylated PIMs), and diacyl-PIMs (Ac_2PIMs, i.e., tetraacylated PIMs).

Supplementary Figure S12 shows the predicted structure of the most abundant monoacyl-PIM_2 (Ac_1PIM_2) detected among the PIMs (see Table 3 in the main text), together with the tandem MS spectrum of this molecular species. An abundant [M-H]- ion at m/z 1455.9478 (calculated 1455.9477 Da) was found in the spectrum (see supplementary Fig S12B and also Table 3). The experimental error range was 0.0011 Da. Other abundant ions in the second MS detector were those at m/z 1171.6751 and 1189.6857, respectively, resulting from the loss of fatty acid at sn-2 , both in the acid form [M-H-RCOOH] and in the form of the corresponding ketene [M-H-RCH=CO], respectively (see legend to the Figure S12 for details).

Using the [M-H-acylmannose]- ion type, fatty acyl(s) on the 2-O-mannose can be identified in the second MS spectrum. The fragmentation pathway of the ions in tandem MS is shown in Fig. S12A. Stearoyl substituent esterified probably on mannose 2 and was recognized by the presence of the ion at m/z 831.3785, see tandem MS in Fig. S12B. This ion arises from loss of the diacylglycerol and confirms the presence of 18:0-fatty acyl substituent as the glycoside. Further, ions at m/z 1293.8938 (1455.9466-162.0528) and at m/z 1027.6328 (1455.9466-428.3138), arising from losses of a mannosyl and a stearoyl-mannosyl moiety, respectively, were identified in the spectrum (Fig. S12B).

Supplementary tables

Table S1 (provided as a separate Excel file)

Primary data, ICP standard analyses results, NGS sequencing data and regression analyses between nutrient concentrations and biomass of shoots and roots

Table S2

Mean values of the C and N concentrations in the dry samples derived from the *Rhizophagus irregularis* biomass produced *in vitro*

Sample	C concentration (%)	N concentration (%)	number of replicate samples
Untreated fungal biomass	54.12	1.491	8
After lipid extraction with chloroform-methanol (2:1, v:v)	39.05	3.692	4
After alkaline lysis of the previous material	35.93	5.327	2

Table S3

Amounts of *N*,*N*′-diacetylchitobiose detected in the samples subjected to chitinase treatment after 24, 48, and 72 hours of incubation. Numbers are means of two technical replicates, and represent peak size (mAU s^{-1}) normalized per mg of dry weight of material subjected to the treatment.

Material	**24 h**	**48 h**	**72 h**
Rhizophagus irregularis cell walls	893	1197	2190
crab-shell chitin	2249	762	5202
Zygorrhynchus sp. cell walls	4891	7283	5707

Table S4

Amounts of *N*, *N*′, *N*′′-triacetylchitotriose detected in the samples subjected to chitinase treatment after 24, 48, and 72 hours of incubation. Numbers are means of two technical replicates, and represent peak size (mAU s^{-1}) normalized per mg of dry weight of material subjected to the treatment.

Material	**24h**	**48h**	**72h**
Rhizophagus irregularis cell walls	810	Not detected	5063
crab-shell chitin	674	886	1810
Zygorrhynchus sp. cell walls	188	755	1177

Supplementary figures

Figure S1

Microphotograph of living (A) and dead (B) biomass of the arbuscular mycorrhizal fungus (*in vitro* produced hyphae and spores of *Rhizophagus irregularis* SYM5) applied to experimental pots in the respective inoculation treatments.

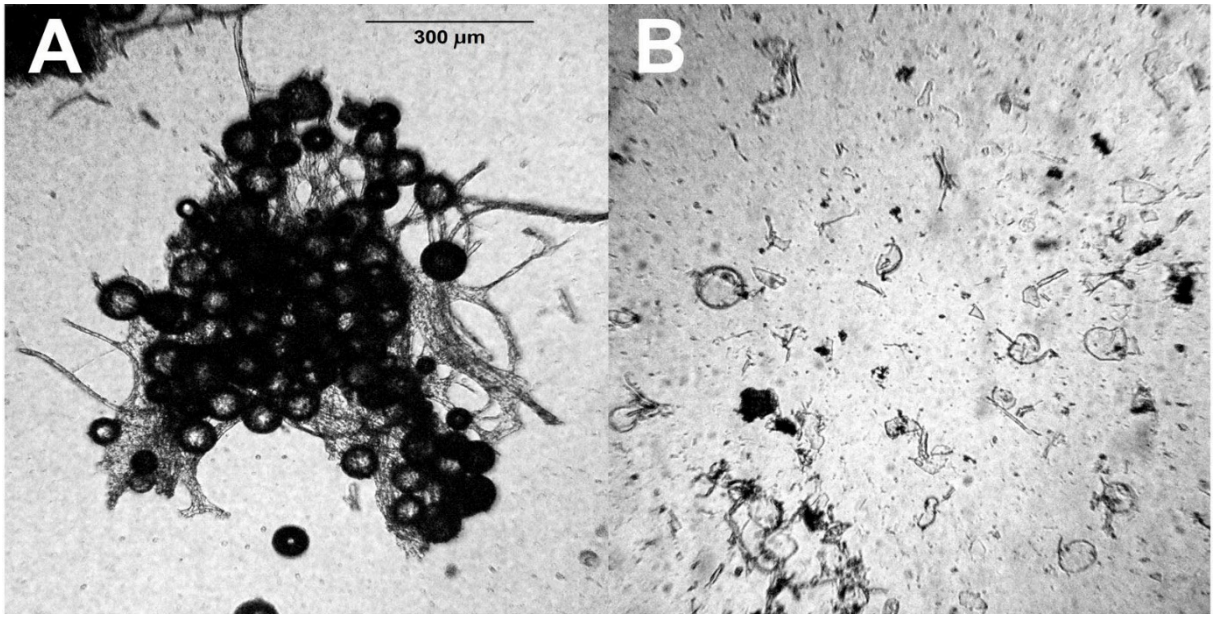

Figure S2

Relationships between macronutrient concentrations within and the biomass of shoots and roots of the experimental plants across the different experimental treatments. Significant linear regressions are indicated by the p – values shown in red. A significant positive relationship indicates that a particular nutrient is possibly growth-limiting according to the framework by Agren et al. (2012), whereas negative regressions indicate dilution effects of growth non-limiting nutrients.

Shoots

Roots

Nitrogen

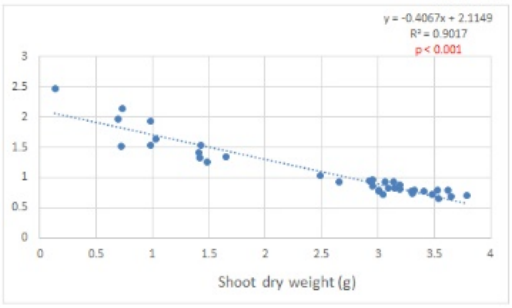

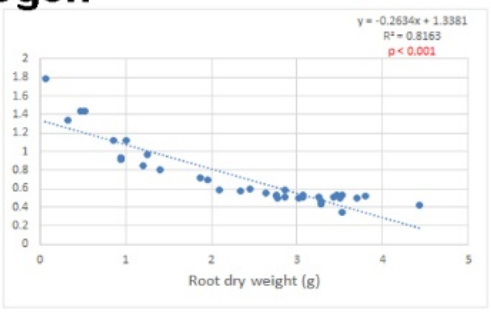

Phosphorus

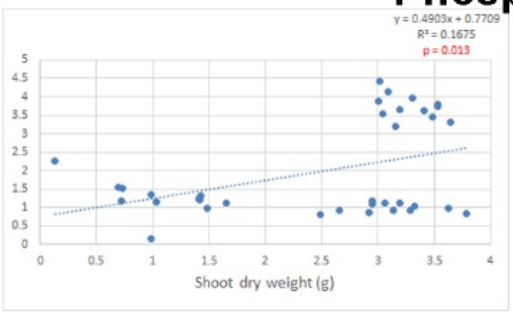

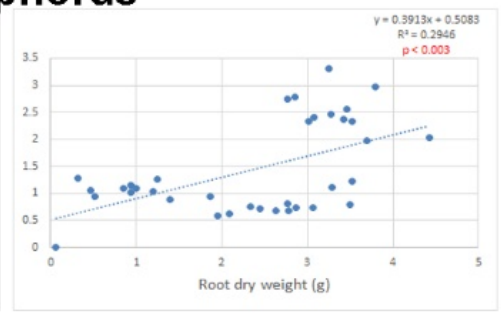

Magnesium

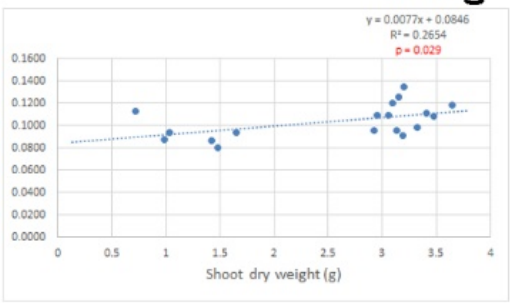

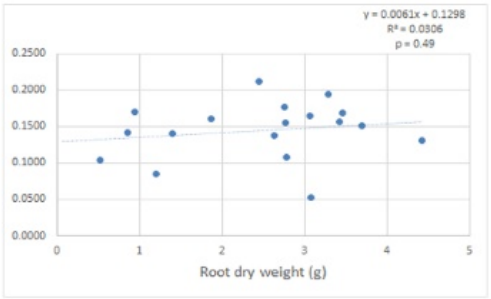

Potassium

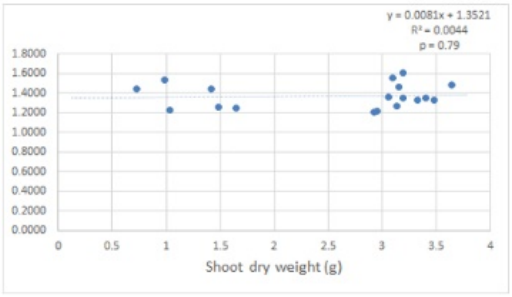

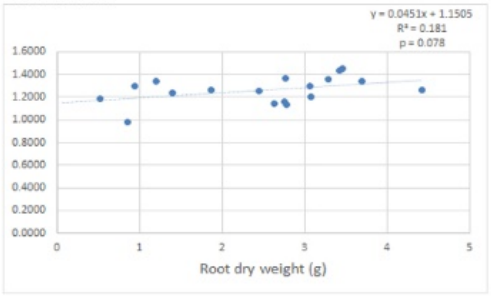

Calcium

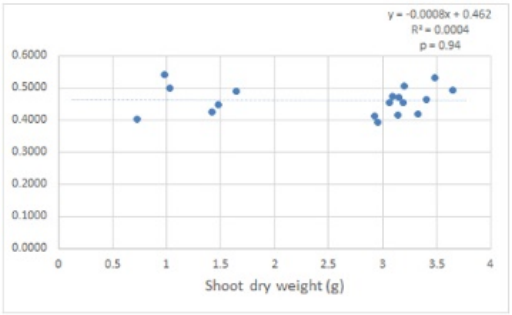

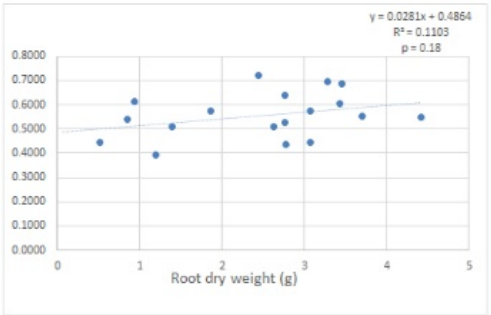

Figure S3

Relationships between micronutrient concentrations within and the biomass of shoots and roots of the experimental plants across the different experimental treatments. Significant regressions are indicated by the p – value shown in red. A significant positive relationship indicates that a particular nutrient is possibly growth-limiting according to the framework by Agren et al. (2012), whereas negative regressions indicate dilution effect of growth non-limiting nutrients.

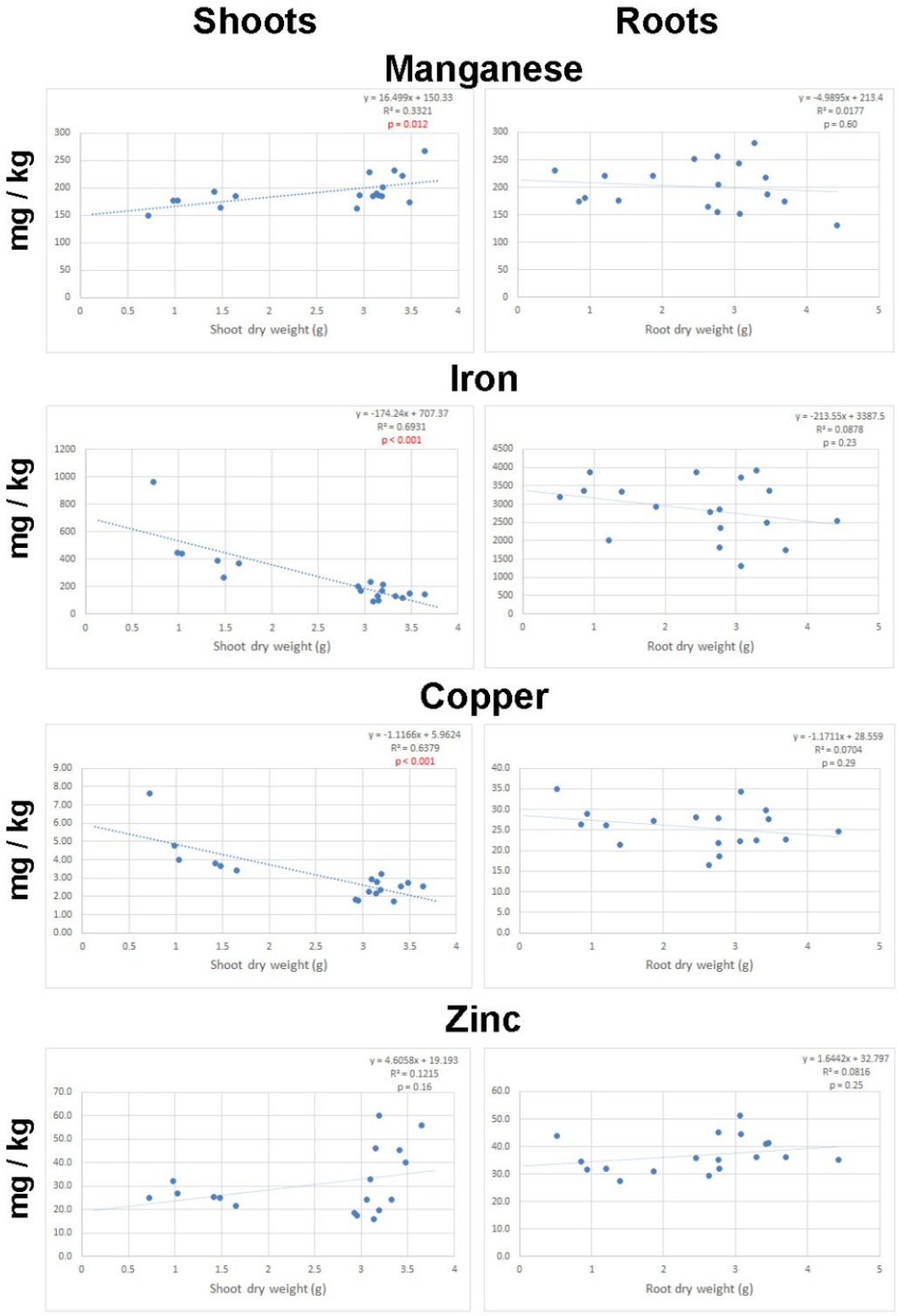

Figure S4

Composition of prokaryotic communities in the potting substrate and in the roots of *Andropogon gerardii* plants as affected by inoculation of the substrate with living arbuscular mycorrhizal (AM) fungus (Living), AM fungal necromass (Dead) and compared with the non-inoculated control (Control). Relative abundances of prokaryotic phyla in the communities are shown (mean values of 11 or 12 replicates per treatment) as per amplicon sequencing. Plastid and mitochondrial sequences were removed from the dataset and then the sequencing data were resampled to achieve comparable sequencing depth for all individual samples before the analysis.

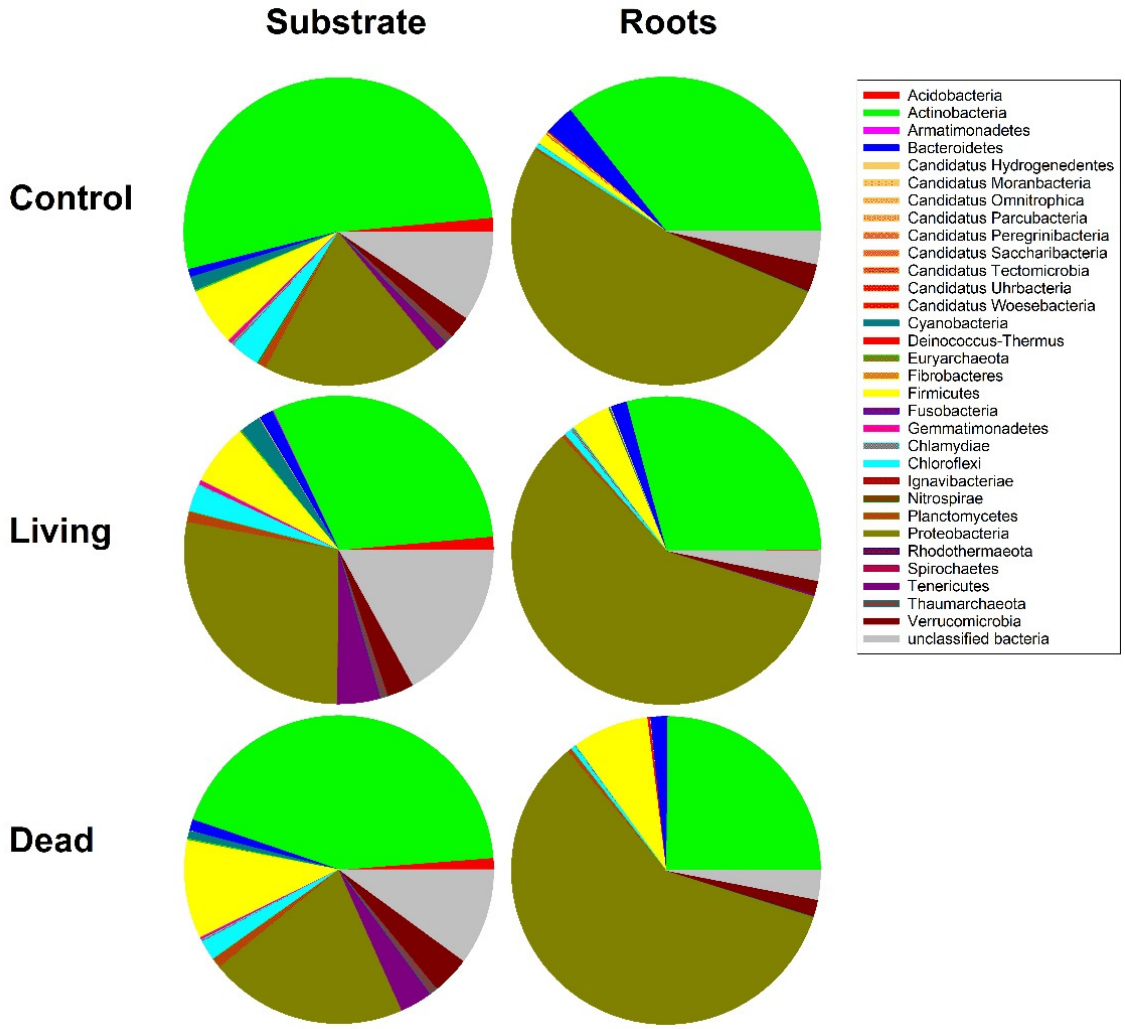

Figure S5

Composition of fungal communities in the potting substrate and in the roots of *Andropogon gerardii* plants as affected by inoculation of the substrate with living arbuscular mycorrhizal (AM) fungus (Living), AM fungal necross (Dead) and compared with the non-inoculated control (Control). Relative abundances of fungal classes are shown (mean values of 11 or 12 replicates per treatment) as per amplicon sequencing. Glomeromycotan and non-fungal sequences were removed from the dataset and then the sequencing data were resampled to achieve comparable sequencing depth for all individual samples before the analysis.

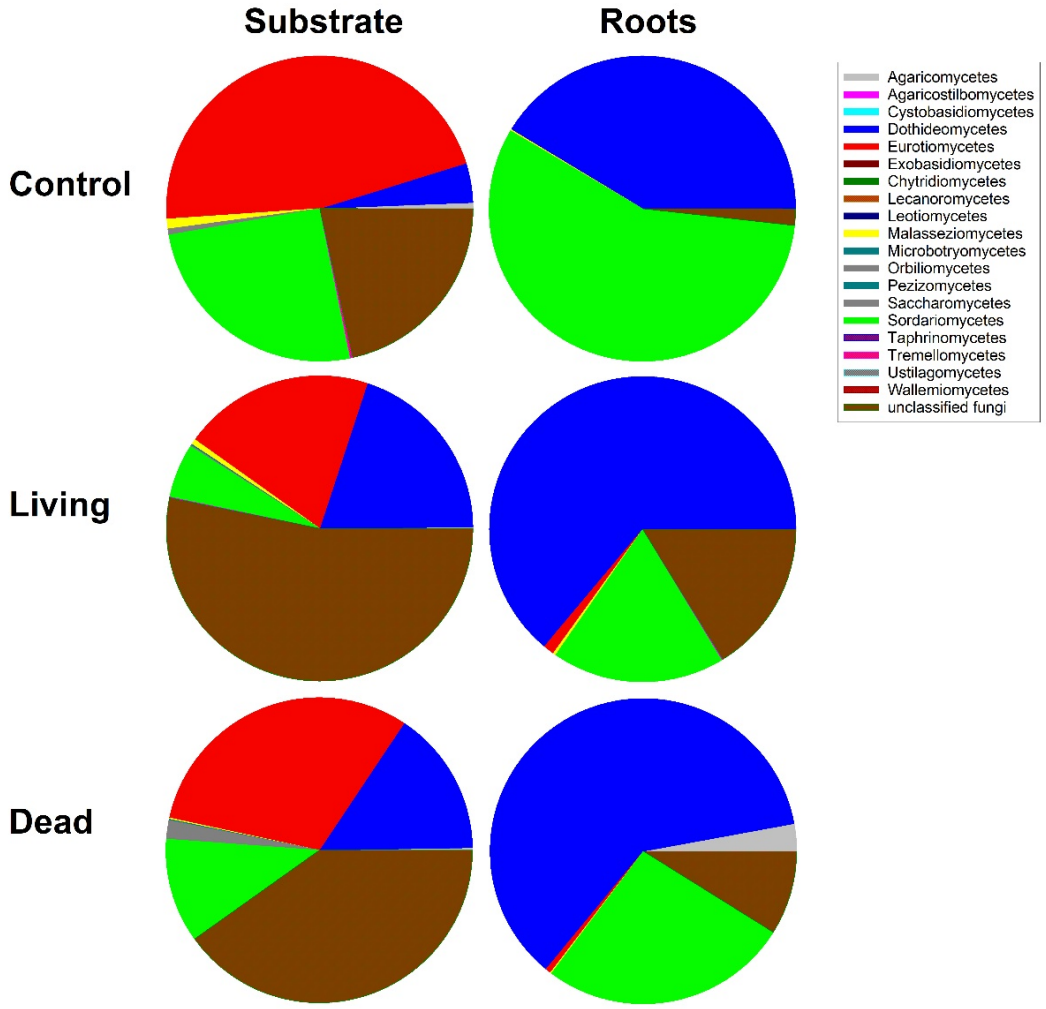

Figure S6

Comparison of prokaryotic (A, C) and fungal (B, D) communities in pots either amended or not with living arbuscular mycorrhizal (AM) fungus *Rhizophagus irregularis* (Living), or amended with AM fungal necromass (Dead) as compared to non-inoculated control treatment (Control), using amplicon sequencing data from 11 or 12 true replicates (pots) per treatment. Results of redundancy analysis (RDA, ter Braak & Šmilauer 2018) are shown, using log(x+1) transformed counts of sequence reads per sample. Community analyses for substrate and root samples from each pot were conducted separately, rarefied to achieve the same sequencing depth per sample (Gryndler et al. 2018), and samples from each pot permuted together in the RDA analysis, using a covariate to remove systematic differences between the two sample sources (substrate and roots). Analyses were carried out either with all three inoculation treatments (A, B), or only with the two treatments amended either with living or with dead AM fungal biomass (C-D). The analyses were carried out with quantitative data at a high taxonomic level, i.e., phyla (32 groups) for prokaryotes or classes (20 groups) for fungi. Blue triangles represent treatment centroids. Percent values indicate share of dataset variability explained by the corresponding constrained axes. All RDA models were statistically significant ($p < 0.05$) for tests of differences between experimental treatments.

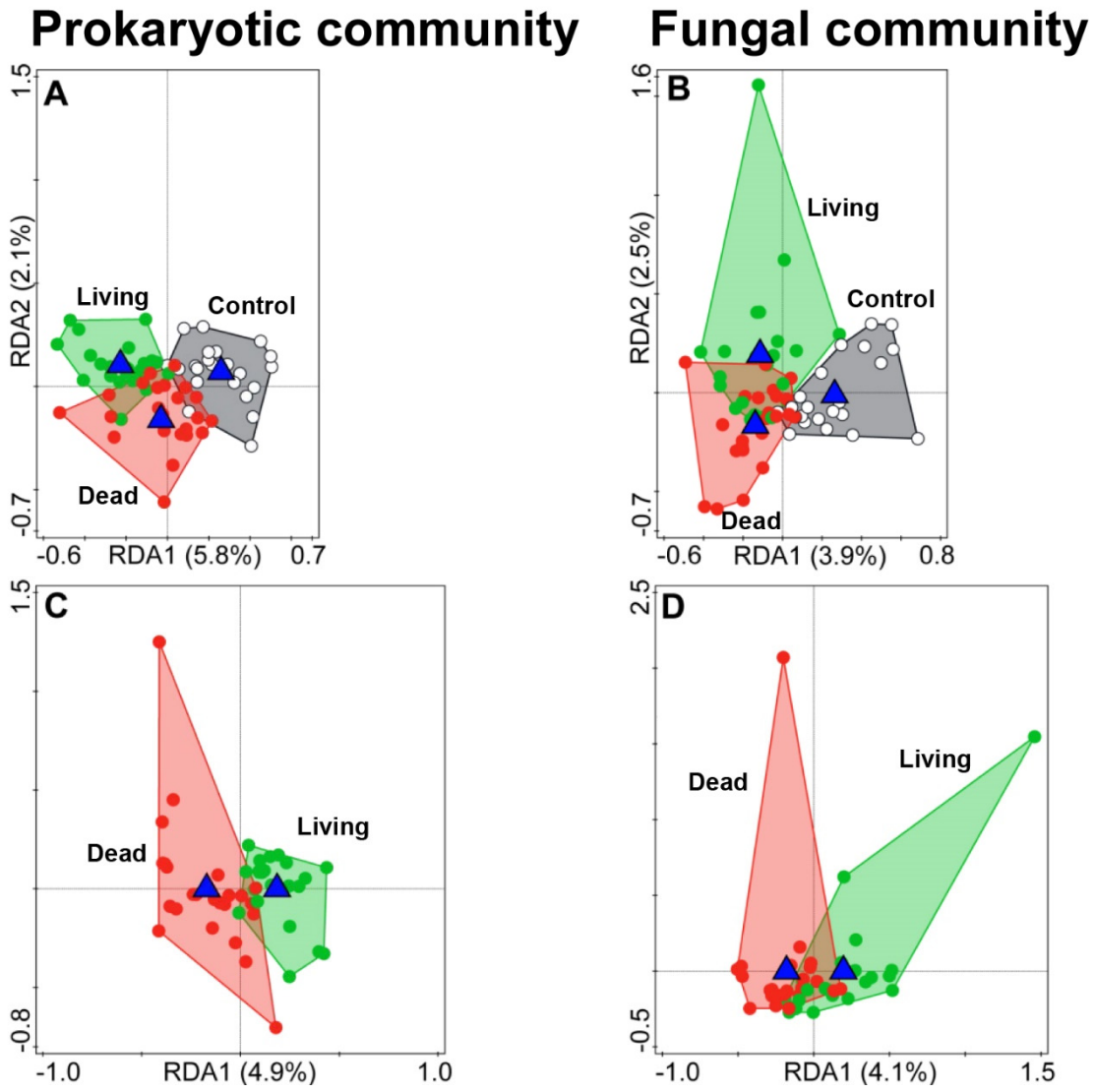

Figure S7

FTIR spectra of standard materials containing amino-groups show typical twin-peak pattern in the region between 1700 and 1450 wave numbers cm^{-1}.

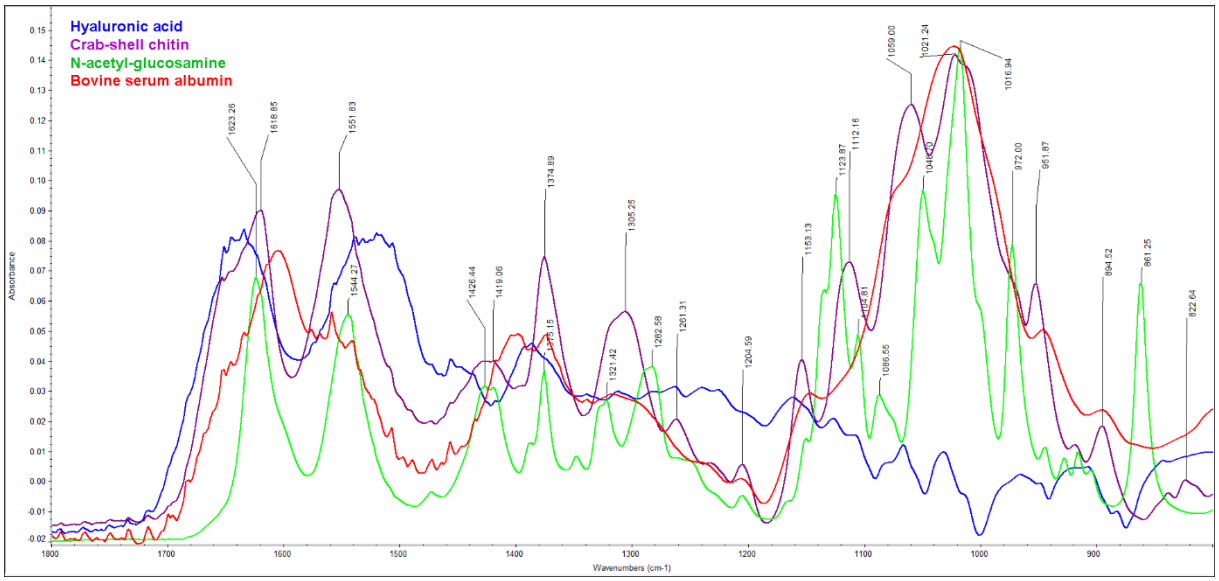

Figure S8

Comparison of FTIR spectra of crab-shell chitin and *Zygorrhynchus* sp. cell walls rich in chitin with *Rhizophagus irregularis* biomass after lipid extraction and after further alkaline lysis, indicating an increasing proportion of chitin (more prominent twin-peak pattern in the region between 1700 and 1450 wave numbers cm^{-1}) in the further-processed mycorrhizal fungal biomass.

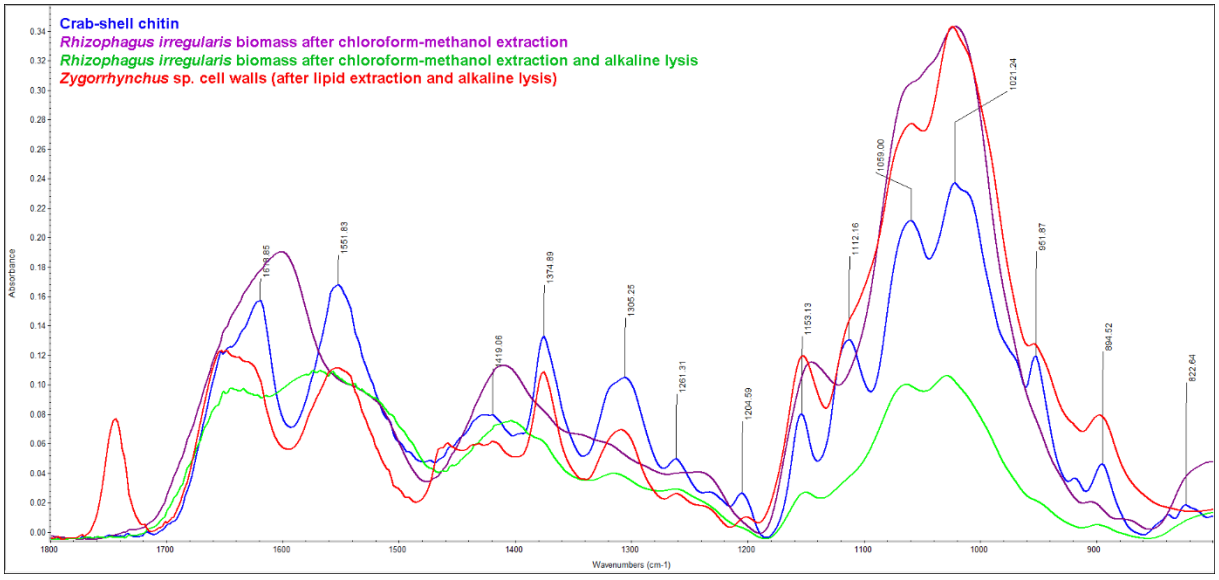

Figure S9

Comparison of FTIR spectra of fully processed *Rhizophagus irregularis* biomass (i.e., after lipid extraction and after alkaline lysis), as compared to crab-shell chitin and cellulose.

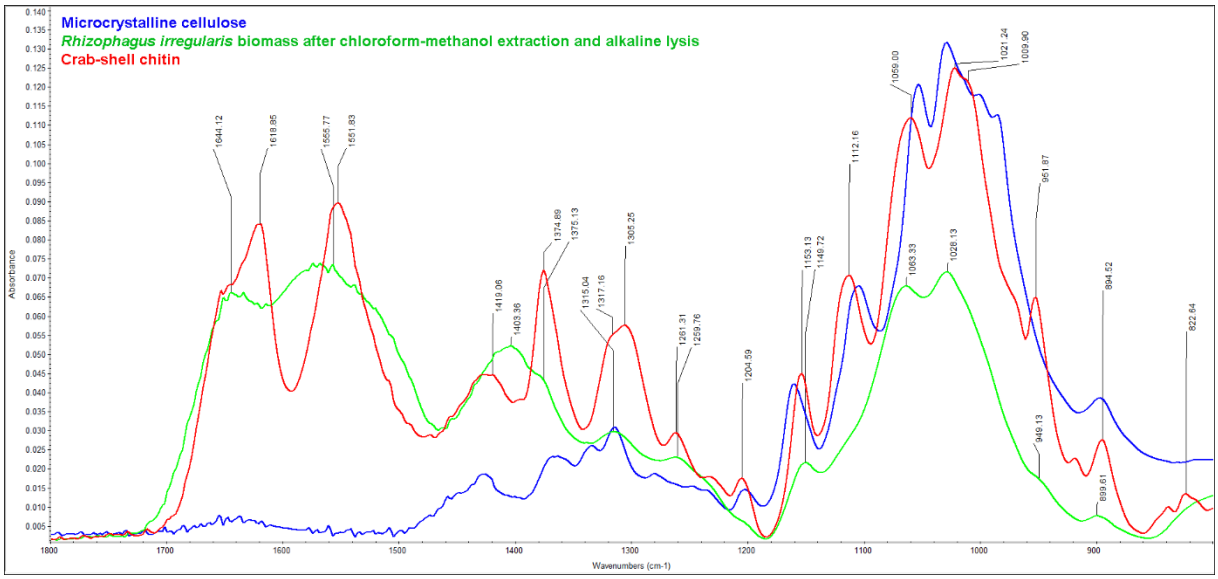

Figure S10

Mass spectrum of *N*,*N*´-diacetylchitobiose from *Rhizophagus irregularis* (positive and negative modes above and below, respectively). Molecular masses of 425+ correspond to [M+H]+, 447+ to [M+Na]+, 423- to [M-H]-, 459- to [M+Cl]-, and 469- to [M+HCOO]- molecular ions

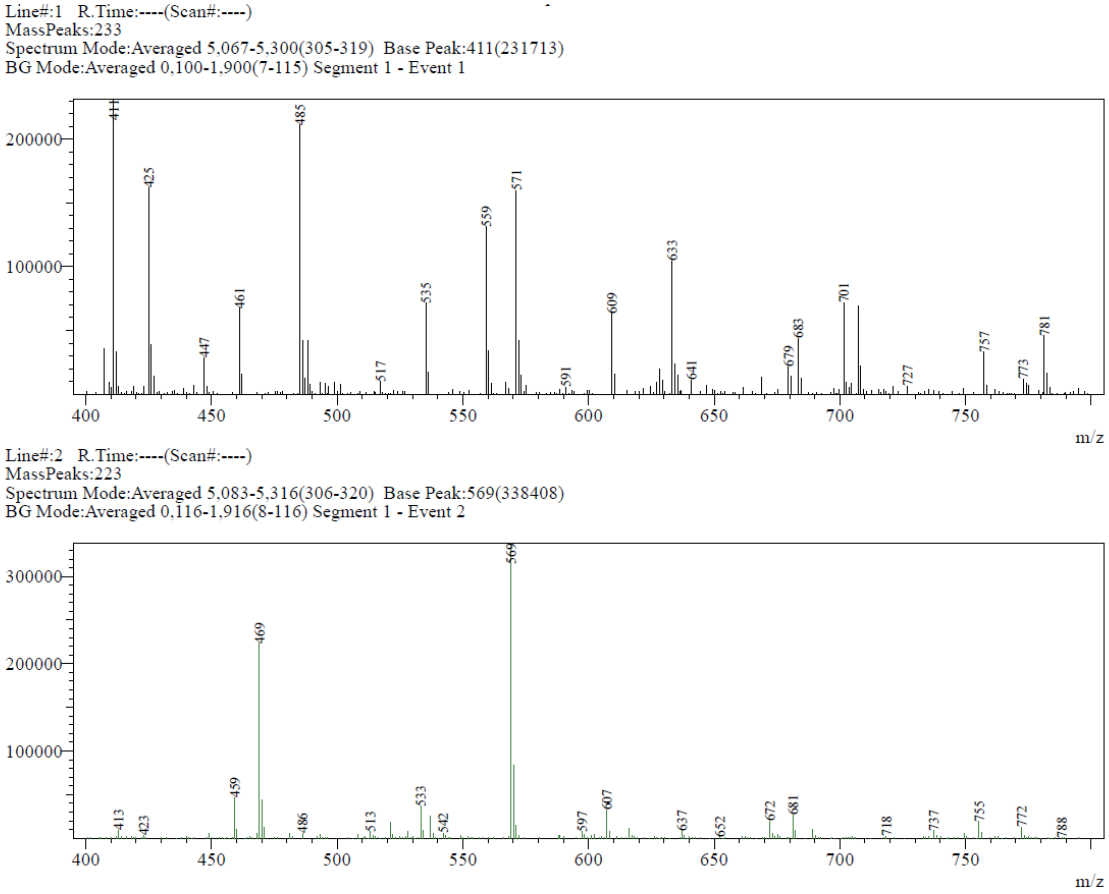

Figure S11

Mass spectrum of *N*, *N´*, *N´´*-triacetylchitotriose from *Rhizophagus irregularis* (positive and negative modes above and below, respectively). Molecular masses of 628+ correspond to [M+H]+, 626- to [M-H]-, and 672- to [M+HCOO]- molecular ions

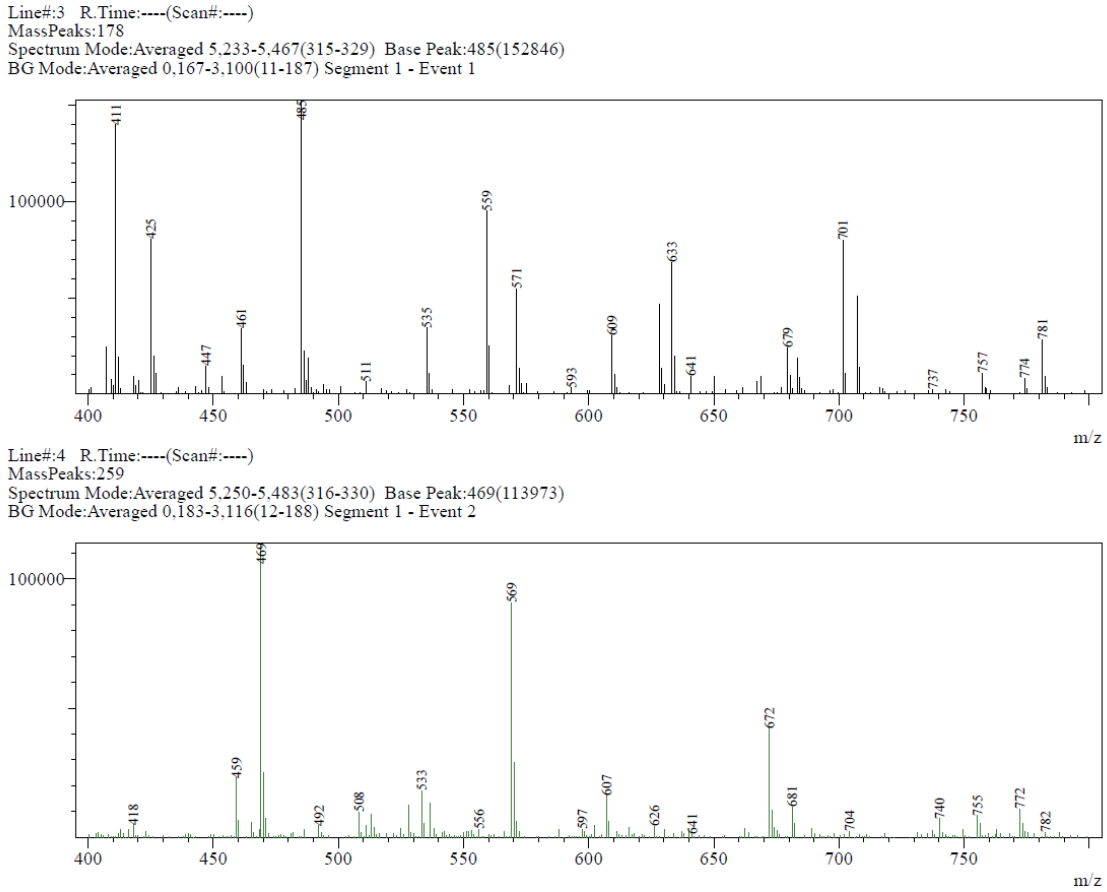

Figure S12

Molecular structure of an abundant monoacyl-phosphatidyl-myo-inositol dimannoside (A) detected in the methanolic extract of *Rhizophagus irregularis* biomass using shotgun mass spectrometry (MS), showing predicted fragmentation sites in the molecule and the resulting tandem MS spectrum (B).

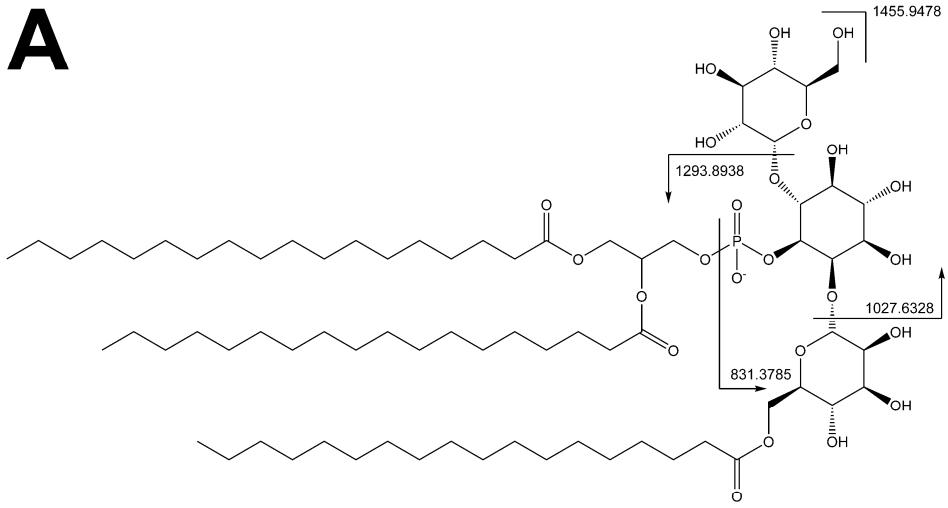

Supplementary references:

Agren GI, Wetterstedt JAM, Billberger MFK (2012) Nutrient limitation on terrestrial plant growth - modeling the interaction between nitrogen and phosphorus. New Phytol 194:953-960. doi:10.1111/j.1469-8137.2012.04116.x

Bernal-Ballen A, Lopez-Garcia J-A, Ozaltin K (2019) (PVA/Chitosan/Fucoidan)-Ampicillin: A bioartificial polymeric material with combined properties in cell regeneration and potential antibacterial features. Polymers 11:1325.

Bojarová P, Chytil P, Mikulová B, Bumba L, Konefal R, Pelantová H, Krejzová J, Slámová K, Petrásková L, Kotrchová L, Cvačka J, Etrych T, Křen V (2017). Glycan-decorated HPMA copolymers as high-affinity lectin ligands. Polym Chem 8:2647-2658.

Bukovská P, Bonkowski M, Konvalinková T, Beskid O, Hujslová M, Püschel D, Řezáčová V, Gutiérrez-Núñez MS, Gryndler M, Jansa J (2018) Utilization of organic nitrogen by arbuscular mycorrhizal fungi - is there a specific role for protists and ammonia oxidizers? Mycorrhiza 28:269-283.

Cranenbrouck S, Voets L, Bivort C, Renard L, Strullu D-G, Declerck S (2005) Methodologies for *in vitro* cultivation of arbuscular mycorrhizal fungi with root organs. In: S. Declerck, D.-G. Strullu, J.-A. Fortin (eds.), *In vitro* culture of mycorrhizas. Springer, Heidelberg. pp. 341-375.

Folch J, Lees M, Stanley GHS (1957) A simple method for the isolation and purification of total lipides from animal tissues. J Biol Chem 226:497-509.

Gryndler M, Šmilauer P, Püschel D, Bukovská P, Hršelová H, Hujslová M, Gryndlerová H, Beskid O, Konvalinková T, Jansa J. (2018) Appropriate nonmycorrhizal controls in arbuscular mycorrhiza research: a microbiome perspective. Mycorrhiza 28:435-450.

Hsu FF, Turk J, Owens RM, Rhoades ER, Russell DG (2007a) Structural characterization of phosphatidyl-myo-inositol mannosides from *Mycobacterium bovis* Bacillus Calmette Guérin by multiple-stage quadrupole ion-trap mass spectrometry with electrospray ionization. I. PIMs and lyso-PIMs. J Am Soc Mass Spectrom 18:466-478 doi:10.1016/j.jasms.2006.10.012

Hsu FF, Turk J, Owens RM, Rhoades ER, Russell DG (2007b) Structural characterization of phosphatidyl-myo-inositol mannosides from *Mycobacterium bovis* Bacillus Calmette Guérin by multiple-stage quadrupole ion-trap mass spectrometry with electrospray ionization. II. Monoacyl- and diacyl-PIMs. J Am Soc Mass Spectrom 18:479-492 doi:10.1016/j.jasms.2006.10.020

ter Braak CJF, Šmilauer P. (2018) Canoco reference manual and user's guide: software for ordination, version 5.10. Microcomputer Power: Ithaca NY, USA.